

DEVELOPMENT OF STRONTIUM FERRITE/POLYAMIDE 12 COMPOSITES FOR  
MAGNETIC DEVICES USING ADDITIVE MANUFACTURING

by

Maria Camila Belduque Correa, B.S.

A thesis submitted to the Graduate Council of  
Texas State University in partial fulfillment  
of the requirements for the degree of  
Master of Science  
with a Major in Engineering  
May 2021

Committee Members:

Jitendra S. Tate, Chair

Wilhelmus J. Geerts

Harold Stern

**COPYRIGHT**

by

Maria Camila Belduque Correa

2021

## **FAIR USE AND AUTHOR'S PERMISSION STATEMENT**

### **Fair Use**

This work is protected by the Copyright Laws of the United States (Public Law 94-553, section 107). Consistent with fair use as defined in the Copyright Laws, brief quotations from this material are allowed with proper acknowledgement. Use of this material for financial gain without the author's express written permission is not allowed.

### **Duplication Permission**

As the copyright holder of this work I, Maria Camila Belduque Correa, authorize duplication of this work, in whole or in part, for educational or scholarly purposes only

## **ACKNOWLEDGEMENTS**

This accomplishment represents a milestone in my career, God has shown me his grace faithfully in every step and through different ways. Because of that I give him glory and I am eternally grateful. He gave me strong parents, Juliet Correa and William Belduque, that have supported me in every step to achieve my dreams and until today they keep encouraging me to become a successful engineer. I am thankful with Dr. Jitendra Tate, excellent advisor, professor, and person. It has been a great experience to follow him in this stage of my life. Thanks to Dr. Vishu Vishwanatan for his advising and patience, and to Dr. Wilhelmus Geerts for his teachings in physics.

Thanks to Camilo Gelvez, for being my family in the United States and lift my spirit up during the hardest moments. To my sister, Natalia, for being my best friend no matter the distance and one of the motives that lead me to keep working hard.

Thanks to the Graduate College for the financial awards that boosted my studies. To Brian Smith for advising me during the PEO scholarship application. And to PEO, a great organization that made the way smooth for me to get to this point.

## TABLE OF CONTENTS

	<b>Page</b>
ACKNOWLEDGEMENTS .....	iv
LIST OF TABLES .....	vi
LIST OF FIGURES .....	vii
CHAPTER	
1. INTRODUCTION .....	1
1.1. Additive Manufacturing Methods and Magnetic Fillers Used .....	2
1.2. Applications .....	11
1.3. Objectives .....	12
2. EXPERIMENTATION .....	15
2.1. Material System .....	15
2.2. Manufacturing .....	15
2.3. Fused Filament Fabrication .....	18
3. CHARACTERIZATION AND RESULTS .....	20
3.1. Density measurements .....	20
3.2. Scanning Electron Microscope .....	20
3.3. Thermogravimetric Analysis and Differential Scanning Calorimetry .....	23
3.4. Mechanical Properties .....	25
3.5. Magnetic Properties .....	28
4. CONCLUSIONS .....	37
5. FUTURE WORK .....	39
REFERENCES .....	40

## LIST OF TABLES

<b>Table</b>	<b>Page</b>
1. OP-71 and OP-56 Properties.....	15
2. Density measurements of composites and neat PA12 according to ASTM 792.....	20
3. Saturation (Ms), remanence (Mr), squareness (S) and coercivity (Hc) of composites printed with and without the effect of a magnetic field and with two different nozzle sizes.....	32

## LIST OF FIGURES

Figure	Page
1. Crystal structure of NdFeB.....	3
2. SEM analysis on surface finish and magnetic particles dispersion on samples printed via FFF, SLS, SLA, from left to right, respectively.....	5
3. a. NdFeB composites hysteresis loop of FFF, SLS and SLA parts.....	6
4. a. Remanence ( $B_r$ ) properties and b. coercivity ( $\mu_0 H_{cj}$ ) of FFF, SLS and SLA samples.....	6
5. Magnetic performance independency from layer orientation in FFF samples.....	7
6. Density variation in a. NdFeB/PA11 pellets, FFF and injection molded samples.....	7
7. a. Residual flux density of NdFeB powder, FFF, SLS and SLA samples.....	7
8. a. Coercivity values showing a decrease of around 25% in SLS samples attributed to nonuniform microstructure.....	7
9. Strontium ferrite crystal structure by Granados et al., 2016.....	9
10. Hysteresis measurements for isotropic (no external field, $H_0$ ) and anisotropic (maximum external field, $H_{max}$ ) printed magnets in all magnetization directions.....	10
11. Microrobot powered by magnetic actuation to perform different locomotive tasks...11	11
12. Generator built with ferrites Halbach arrays replacing traditional magnets.....	12
13. Magnetic properties of most common magnets.....	14
14. 50wt% NdFeB/PA12 at zero, two and five mixing cycles of three minutes.....	16
15. Process 11 Twin-Screw Extruder and table showing parameters used to create each composite filament and final diameters.....	17
16. Die swell in NdFeB/PA12 filament.....	18

17. CraftBot XL3 feeding zone and OP-56/PA12 buckling between the drive gears.....	19
18. NdFeB, OP-56, and OP-71 in powder form.....	20
19. NdFeB/PA12 on top, OP-56/PA12 in the middle, and OP-71/PA12 in the last row...	22
20. TGA and DSC results on neat PA12 and composites with a 50wt% loading level.....	24
21. Flexural modulus and flexural strength values obtained from the composites manufactured at 50wt% loading levels.....	26
22. Tensile test setting and failure modes of PA12, OP-56/PA12, NdFeB/PA12 and OP-71/PA12.....	27
23. Ultimate Tensile strength and tensile modulus.....	28
24. Printing set up to induce a magnetic field on magnetic filaments.....	29
25. Hysteresis loop of filament composites.....	30
26. Samples on the rod holder. ....	31
27. Hysteresis loops of all composites with and without a magnetic field.....	32
28. PPMS results of NdFeB/PA12.....	34
29. NdFeB/PA12, OP-56/PA12 and OP-71/PA12 SEM image of particles alignment when the materials are printed with the effect of a magnetic field.....	35

## 1. INTRODUCTION

It is clear the rapid growing of composites in all industries, they are replacing traditional material systems in the aerospace, wind energy, automotive, and marine fields. Their high strength to weight ratio and low cost are leading both industrial and academy sectors to keep innovating with solutions that include them. Polymer composites are leading this trend, their properties are highly increased with reinforcements such as carbon or glass fiber, or fillers at the micro and nanoscale size, which have the capacity to enhance a material performance with loading levels as low as 0.5wt%, this is the case of alumina nanoparticles to unsaturated polyester or other matrices for ballistic applications [1, 2]. Fillers can also be used at considerably high concentrations, as is the case of 92wt% of Neodymium Iron Boron (NdFeB) in polyurethane to create lighter magnetic materials [3]. The properties most improved in advanced polymer materials that have reached a commercial level are corrosion, flammability, strength, resistance, tension, and thermal degradation. Furthermore, these materials are compatible with additive manufacturing (AM) processes. Layer by layer methods that reduce waste, processing times, costs, and generate components with outstanding properties and complex structures with the aid of a Computer aided design (CAD) software. To the list of materials that both the AM and polymer composites industries share, bonded magnets are being added. The conventional processes used to manufacture them are injection molding, sintering and compression bonding of NdFeB and hard ferrites filling a thermoplastic or elastomeric matrix. Although the parts product of these methods exhibits a lower maximum energy product and lower operational temperature compared with fully dense magnets, their mechanical properties are outstanding, electrical resistivity is

improved, their magnetic output can be tailored for a given size and/or shape and the structures designs can be complex given the flexibility of the binder.

### **1.1. Additive Manufacturing Methods and Magnetic Fillers Used**

As mentioned, NdFeB and hard ferrites are the common powders employed to create bonded magnets. These materials were adopted to reduce the rare earth elements in magnets, which are expensive and with a limited availability. According to their size, isotropic or anisotropic magnets can be produced. The first being applied mostly to composites which powder size orients the crystal grains in different orientations, whereas anisotropic magnets are the result of single crystals alignment during manufacturing, yielding a higher magnetic flux when the field is applied parallel to such alignment.

NdFeB was introduced to the market in the 80's by General Motors, Sumitomo Special Metals Co., Ltd. and by the U.S. Naval Research Laboratory at almost the same time due to the need of independency of US from external sources of Cobalt to produce SmCo magnets, which became highly expensive after instabilities in Congo, the global provider of around 60% of this material by that time. NdFeB is an intermetallic compound, highly available, recyclable and has an energy density of around 512 kJ/m<sup>3</sup>. NdFeB are classified as permanent/hard magnets, this property highly depends on the microstructure result of the manufacturing process. For instance, a chemical route is not recommended because of its reactivity and highly oxidation behavior [4]. The NdFeB tetragonal crystal structure can be observed in figure 1, it has 68 atoms and 6 crystallographic distinct iron sites per unit cell and its easy magnetic axis can be found along the c-axis [5]. Some of the drawbacks of NdFeB are their low Curie Temperature (T<sub>c</sub>), which goes around 311°C, brittle behavior, and sensitivity to corrosion. However,

their capacity to generate a strong magnetic field in a small volume and availability, place them as the most acquired type of magnets in the world given the increasing demand in renewable energy sources, electric vehicles, and electronics.

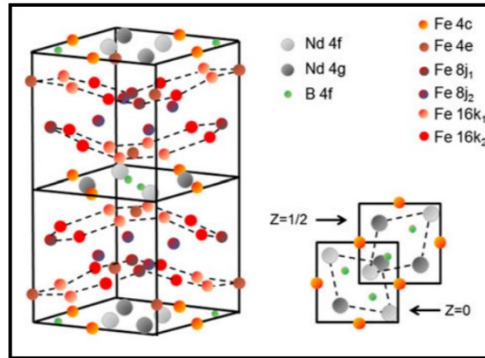


**Figure 1.** Crystal structure of NdFeB.

NdFeB magnets are being actively investigated using different AM processes. For instance, Huber et al., 2020 [6] manufactured a 5 x 5 x 5 mm magnet through Stereolithography (SLA) by using a composite of 92wt% of NdFeB powders and a methacrylate resin obtained via centrifugal mixing. The same design was printed via selective laser sintering (SLS) and fused filament fabrication (FFF) to compare the magnetic properties obtained through each method.

SLA is one of the first AM methods to be developed, it consists of lithography and printing of 2D parts and their extension to the third dimension through photopolymerization. This process occurs with the application of UV radiation, X-ray, electron beam or visible light – according to the application – to a specific part of the bulk material, which is poured over a platform bed in layers of very thin sizes. Common materials are polymer resins, radiation curable resins, photopolymers and hydrogels [7]. A layer of 60  $\mu\text{m}$  is created in this case. Subsequently, the platform bed is lowered, and the heat of the laser is applied again until the part is complete.

In contrast, SLS does not need a binder to print parts. Basically, it consists of

spreading metals, ceramics, polymers, or composite powders, in this case NdFeB powders, on a bed placed inside a nitrogen-gas chamber. A CO<sub>2</sub> laser beam will fuse specific parts of the powder bed below the melting point of the material and according to the CAD design, layers of 0.075mm-0.1mm thick are formed, in this study 100 μm. Successively, the platform is lowered, more material is spread over with a counter rotating powder leveling roller to manufacture the next layer, and the process is repeated until the final part is complete. It is worth to mention that unfused powder serves as support for the 3D printed part, a disadvantage of the SLA process [8]. This method does not melt the material, which reduces microstructural modifications. Therefore, the maximum energy product, or the maximum magnetic strength that it can store, is also conserved.

Regarding the FFF process, the authors used a compound with 89wt% of the same NdFeB powder inside a Polyamide 11 (PA11, Nylon 11) matrix and create a filament of 1.75mm using a twin-screw extruder. Compared with Acrylonitrile butadiene styrene (ABS) and Polylactic acid (PLA), nylons are characterized because of their high melt flowability, which allows them to be filled with approximately 60wt%-80wt% loading level of magnetic particles and higher mechanical performance [9]. FFF consists of a nozzle that melts and extrudes layers of commonly 0.2 mm thick on top of a heated bed.

Scanning electron microscope (SEM) analysis is conducted on the samples, which did not receive post-processing, to observe and compare the surface finish and layer structure obtained through each AM method. Below the SEM images showed in figure 2 there is a graphic description of FFF, SLS and SLA methods courtesy from Huber et al., 2020. Regarding surface finish, the SLA results are the most promising, whereas FFF

seems to yield a higher roughness to the structure, and SLS presents some cracks. These aspects can also be observed in figure 2.

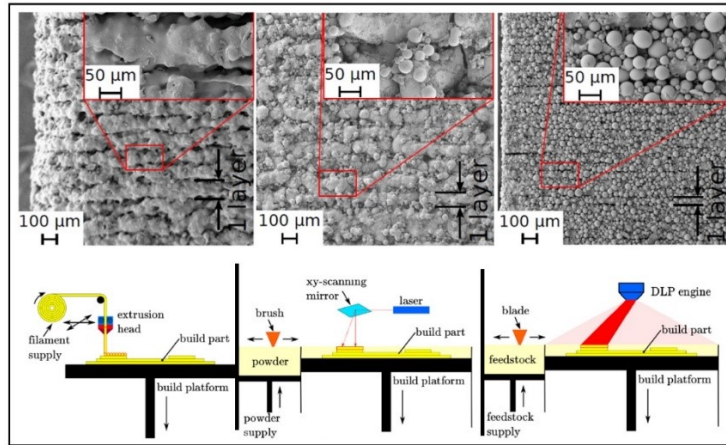


**Figure 2.** SEM analysis on surface finish and magnetic particles dispersion on samples printed via FFF, SLS, SLA, from left to right, respectively. On the lower side, a visual description of each process.

The magnetic measurements results are displayed on figure 3a, and the values of remanence and coercivity in figure 4. The remanence of the SLS sample is higher than that of the FFF and SLA samples, whereas its coercivity is lower compared to FFF and SLA's samples, which yielded better, and almost equal values attributed to uniformity in grain size and distribution. These properties are affected during the melting and fast cooling required by the processes, and can be improved by avoiding the complete melting of the material – i.e. sintering – in order to control easier its microstructure [10]. SLS shows significative results, as observed in figure 3b, where the black curve represents the SLS sample showed on the left, the other specimens correspond to modifications of this sample by infiltrating the eutectic alloys shown to increase the Nd boundary phases and improve coercivity.

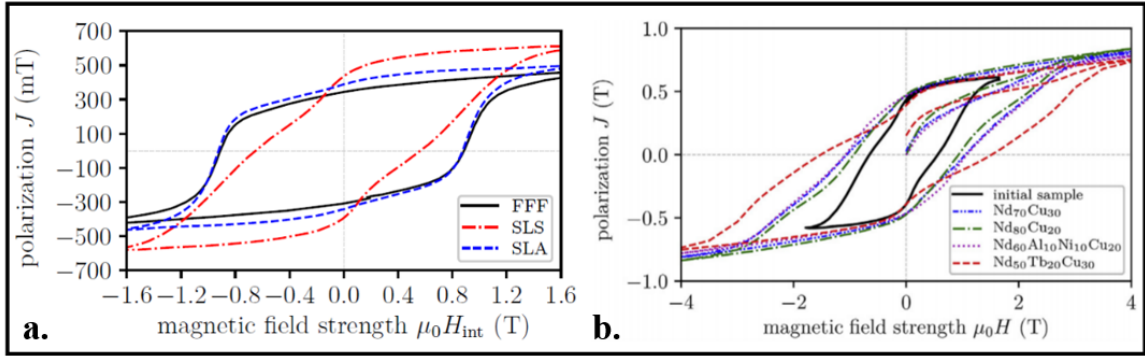


**Figure 3. a.** NdFeB composites hysteresis loop of FFF, SLS and SLA parts. **b.** magnetic behavior of the SLS sample shown on the left figure and other samples modified with eutectic alloys and printed via SLS.

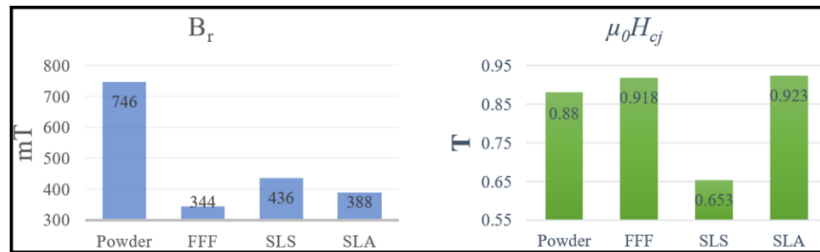


**Figure 4. a.** Remanence ( $B_r$ ) properties and **b.** coercivity ( $\mu_0 H_{cj}$ ) of FFF, SLS and SLA samples.

One of the main parameters of FFF is the layer orientation, the literature reports no effects from it to the magnetic properties when the particles have an isotropic nature, as shown on the left side of Figure 5 obtained from Huber et al., 2016, which also presents the difference in magnetic behavior between NdFeB/PA11 magnets created via injection molding and FFF. On the right side of the same figure, the magnetic behavior of Iron/PLA (by Protopasta) cubic samples is also observed to be almost equal despite the field being applied in different directions [11]. The magnetic particle size used for both experiments are 50  $\mu\text{m}$  and 40  $\mu\text{m}$ , respectively.

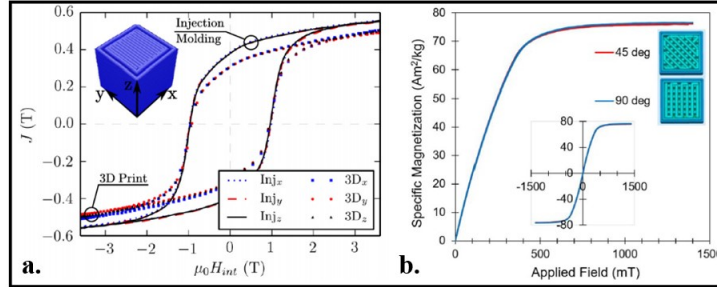


**Figure 5.** Magnetic performance independency from layer orientation in FFF samples. **a.** NdFeB/PA11 FFF and injection molding cubic samples. And **b.** Iron/PLA cubic samples.

It must be noted that AM methods highly affect the final part density, and consequently, the magnetic performance of the resulted parts. From the studies summarized above, it is concluded that FFF decreases this characteristic at significant levels compared to SLS, SLA and injection molding as shown in figure 6. Figures 7 and 8 display the remanence and coercivity values obtained for both studies.

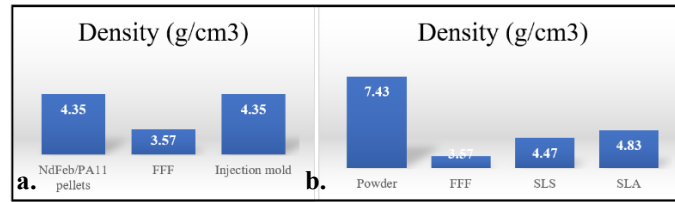


**Figure 6.** Density variation in **a.** NdFeB/PA11 pellets, FFF and injection molded samples. And **b.** powder, FFF, SLS and SLA composites of NdFeB.

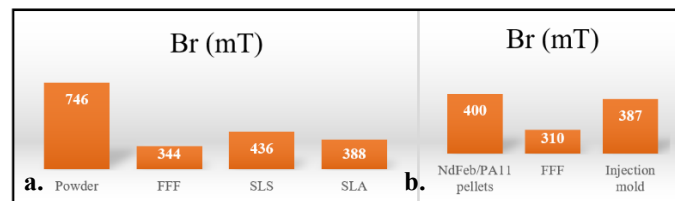


**Figure 7. a.** Residual flux density of NdFeB powder, FFF, SLS and SLA samples. **b.** Residual flux density of NdFeB /PA11 pellets, FFF and injection molded samples.

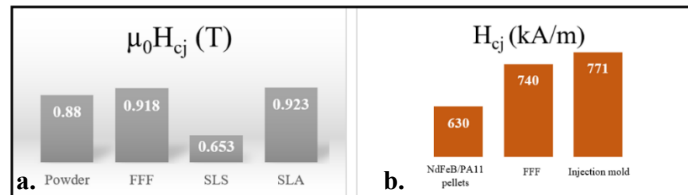


**Figure 8. a.** Coercivity values showing a decrease of around 25% in SLS samples attributed to nonuniform microstructure. **b.** Intrinsic coercivity of NdFeB/PA11 composites.

Another common type of magnetic particles are Iron-oxides such as magnetite ( $\text{Fe}_3\text{O}_4$ ) and maghemite ( $\gamma\text{-Fe}_2\text{O}_3$ ), which have a saturation magnetization of around 80–100  $\text{A}\cdot\text{m}^2\text{kg}^{-1}$ , the highest values among iron-oxides [12]. They are mostly used in biomedical applications because of their low toxicity, ease of processability and superparamagnetic behavior at room temperature. This last property is mostly attributed to the size of a single domain particle – i.e., a particle with a uniform magnetization – which is around 50nm [13]. Strontium ferrite ( $\text{SrFe}_{12}\text{O}_{19}$ ), Barium and Cobalt powders are becoming highly implemented for AM as well. These particles are obtained through powder metallurgical methods and yield magnetic moment densities that are lower than those of Iron and rare earth magnets, but their magnetic hysteresis is in between soft magnetic iron and hard magnetic NdFeB. Typical values for remanence, coercivity, and energy product of SrFeO are:

$$B_r = 0.36 \text{ T Residual magnetic flux density}$$

$$H_{ci} \geq 320 \text{ kA/m intrinsic coercivity}$$

$$(BH)_{\max} = 25000 \text{ T} \cdot \text{A/m maximum energy product}$$

Ferrites are not susceptible to oxidation or corrosion, which extends their magnetic properties for longer periods of time. They are low-cost and easily found in single domain sizes of around 1.5  $\mu\text{m}$ , a highly attractive characteristic to obtain anisotropic magnetism [14, 15], which can also be understood as the preferred orientation, or easy axis, at which all the domains align. The anisotropy in a magnetic material is the result of either its crystal structure, shape, stress, annealing, deformation or irradiation, or exchange anisotropy [16]. In  $\text{SrFe}_{12}\text{O}_{19}$ , this behavior is attributed to its crystal structure, which crystalline lattice is defined by two parameters:  $a$ , the width of

the hexagonal plane, and  $c$ , the height of the crystal. Generally, the preferred orientation goes parallel to  $c$ . the hard axis goes along the basal plane.

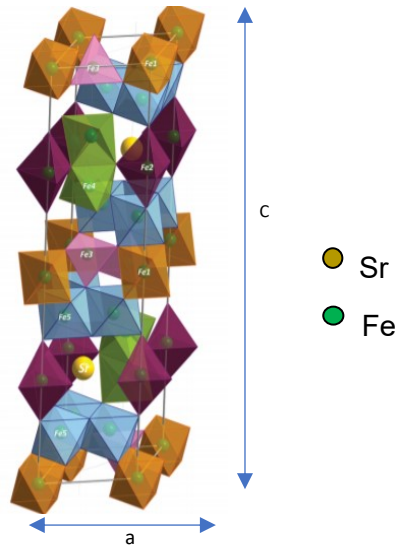


**Figure 9.** Strontium ferrite crystal structure by Granados et al., 2016 [17]

Outstanding magnetic properties are not the only attributes desired in polymer composites filled with ferrites. For instance, Hanemann et al., 2020 [18] investigated the mechanical properties of Barium ferrites and ABS. They obtained a reduction in the tensile strength, ultimate stress, and ultimate strain, of such composites at different loading levels. These results were attributed to the fillers acting as discontinuities and a low 3D printing quality creating voids. Consequently, decreasing the material's magnetic behavior. In polymer composites is crucial to guarantee a good adhesion that allows the fillers to support most of the applied load before transferring it to the matrix and fail. This depends on the chemical characteristics of both components and can be improved with agents in some cases[2]. Additionally, the machine used to obtain the filaments for FFF highly influences their quality in terms of voids. For example, twin screw extruders have two co-rotating screws that improve dispersion and reduce the shear in the polymer

during the different thermal stages that it undergoes from the cooling zone to the die. Furthermore, they are equipped with vacuum systems to remove contaminants and air. On the opposite side, single screw extruders do not have vacuum systems, and the screw induces a high shear rate, limiting the materials that can be manufactured and their quality [19].

Huber et al., 2020 [20] investigated the mechanical and magnetic properties of strontium ferrite/PA12 composites, they found a decrease in the tensile stress as the filler content (up to 55vol%) increased, however, the tensile strain at break increased considerably. Regarding its magnetic properties, cubic samples were printed without an external field and under the effect of an external field to obtain magnetically anisotropy samples. The remanence values for the latter were 40% higher than those of the isotropic samples, whereas the coercivity of the same specimens decreased. Figure 10 shows the hysteresis loop of these materials increasing in area and adopting a squared shape when they are under the effect of the magnetic field. This squareness is also observed to improve with higher filler concentration.

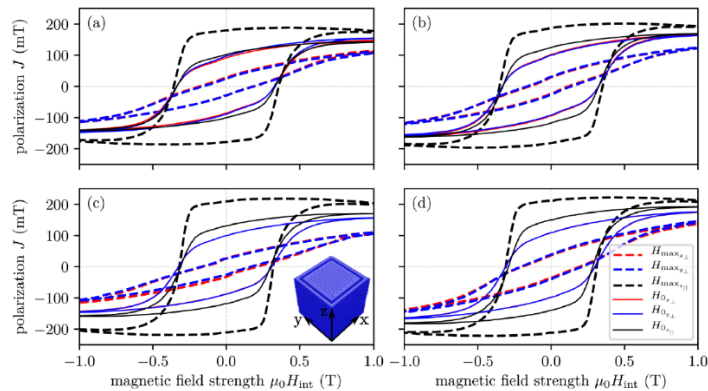


**Figure 10.** Hysteresis measurements for isotropic (no external field,  $H_0$ ) and anisotropic (maximum external field,  $H_{max}$ ) printed magnets in all magnetization directions. Filling fraction: (a) 40 vol%, (b) 45 vol%, (c) 50 vol%, and (d) 55 vol%.

## 1.2. Applications

Magnets are already employed in different industries such as electronics, power generation, medical devices etc. However, with the advancement of technology science is looking to expand the reach of these materials and innovate, or improve them for the same purposes by, for example, decreasing their weight and costs, and obtaining complex shapes with reduced or no assembly operations.

One of the potential applications of bonded magnets for medical applications is drug delivery robots. Wenqi Hu et al., 2018 [21] processed a microrobot of silicone elastomer filled with NdFeB controlled by magnetic actuation to perform different locomotive tasks that include pick up and release objects and avoid obstacles. Figure 11 displays this behavior in a simulated stomach along with the ultrasound image and the gripping movement.

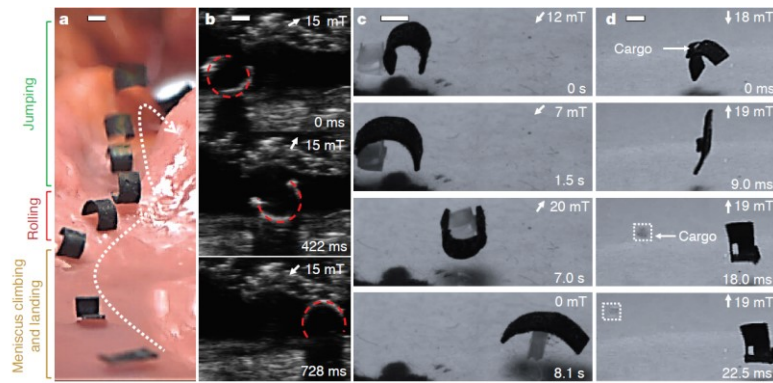


**Figure 11.** Microrobot powered by magnetic actuation to perform different locomotive tasks.

Iqbal et al., 2019 explored  $\text{SrFe}_{12}\text{O}_{19}$ /Polythiophene for electromagnetic applications. The shielding effectiveness of these materials proved to be larger compared to that of the full density strontium ferrite. This result is attributed to the dielectric properties of both the polymer and the reinforcement [22]. In another study, Kallaste et al., 2012 investigated how to replace fully dense magnets with Halbach array made of

strontium ferrite composites for wind generators. This set up maintains the magnetic energy required by the system without increasing the weight. If only strontium ferrite were used, the amount of material needed to generate an energy density compared to that NdFeB would be too large. Although the fabrication of Halbach device is not detailed, FFF can be used to print it by adding an electromagnet with which a printing field can be applied and manipulated into the desired directions [23].

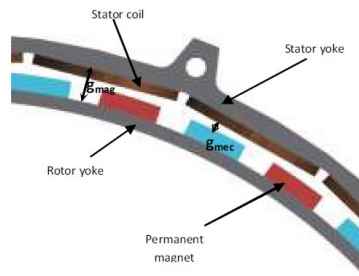


**Figure 12.** Generator built with ferrites Halbach arrays replacing traditional magnets.

### 1.3. Objectives

Currently, work that reports on the magnetic behavior of 3D printed hard magnetic material is scarce. Furthermore, there is no commercially available filament to print permanent magnets. There is only one composite, Iron/PLA by Protopasta, which has been intensively studied. These investigations agree on that PLA is filled with 40wt% of Iron with a particles size of around 40  $\mu\text{m}$  [11]. Mechanically, such material shows a brittle behavior, which highly complicates the 3D printing process. This also means that its magnetic properties are very limited and cannot be placed as an alternative for magnetic/structural applications, a clear example is given in [24], in which a transformer core is 3D printed but its magnetic analysis showed non saturated hysteresis loops.

The main goal of this study is to manufacture NdFeB/PA12 filaments, and two types of SrFe<sub>12</sub>O<sub>19</sub> filaments composites, namely OP-71/PA12 and OP-56/PA12 for fused filament fabrication purposes by using a co-rotating twin screw extruder. FFF is chosen

because, compared to SLS and SLA, it is safer and low cost. Both the materials and process are highly available, which has increased their accessibility by industry, academics and users at home. Furthermore, and most important, FFF can be adapted to print anisotropic magnets, which have better properties than isotropic magnets at the same loading level. To upgrade an SLA or SLS machine to induce a magnetic field during printing has not been explored until now because the laser intensity increases at high magnetic fields. This would result in polymer composites products with weaker performance because of the microstructural changes induced by such intensity, and could represent an operational hazard [25].

$\text{SrFe}_{12}\text{O}_{19}$  has been chosen because of its chemical stability, which allows it to be obtained at dimensions close to the single domain particle size and avoids oxidation issues as encountered in composites using NdFeB particles. Factors such as particle size, shape, loading level and processing temperature will be carefully chosen for the filament manufacturing since these parameters highly affect the magnetic anisotropy and mechanical behavior of 3D printed parts.

Besides showing higher mechanical performance than most of the common plastics used in 3D printing, PA12 is characterized because of its high melt flowability, which allows it to be filled with approximately 60wt%-80wt% loading level of magnetic particles. The advantages of  $\text{SrFe}_{12}\text{O}_{19}$  and NdFeB particles has been explained, an additional comparison of their main properties is shown in figure 13 [26]. A filament composite based on these two types of materials certainly would be implemented for high requirement applications in most industries.

Materials	$B_r$ (mT)	$H_c$ kA/m	$(BH)_{max}$ (kJ/m <sup>3</sup> )
Alnico	650	40-45	42-45
Ferrites	350-400	240-320	27.5-31.5
Sm Co	1050-1150	880-1360	145-160
Nd-Fe-B	1200-1300	800-1200	210-250

**Figure 13.** Magnetic properties of most common magnets.

The shape and size of the magnetic particles, and their distribution in the matrix is analyzed with a JEOL Scanning Electron Microscope. An SDT 650 is employed to perform thermogravimetric analysis (TGA) and Differential Scanning Calorimetry (DSC). A Microsense Vibrating Sample Magnetometer (VSM) is used to understand the magnetic properties of filaments and 3D printed samples deposited with and without an external magnetic field. Lastly, flexure and tension behavior of 3D printed samples is determined according to ASTM D790 and D638.

## 2. EXPERIMENTATION

### 2.1. Material System

Four types of filaments with the same matrix and three different types of magnetic particles are manufactured. Nylon 12 acts as the matrix, it is a powder obtained from Evonik. It has high flowability and chemical stability, which indicates a good capacity to be mixed with other materials and provide a good adhesion. Additionally, Nylon 12 has a low moisture absorption compared to other polyamides.

Strontium ferrite OP-71 and OP-56 from DOWA Electronics Inc are used as fillers at a 50wt%. The following table includes the main properties of these particles given by the manufacturer.

**Table 1.** OP-71 and OP-56 Properties

SrFeO	Remanence [emu/cm <sup>3</sup> ]	Coercivity [Oe]	Density [g/cm <sup>3</sup> ]	Particle size [μm]
OP-71	151	2510.7	3.33	1.5 – 2.5
OP-56	152	3091.3	3.09	1.01

The third filament composite is filled with NdFeB at a 50wt%, it is obtained from Nanochemazone Inc, these particles have a range size from 5 to 10 μm provided by the manufacturer. No information regarding its magnetic properties was given.

### 2.2. Manufacturing

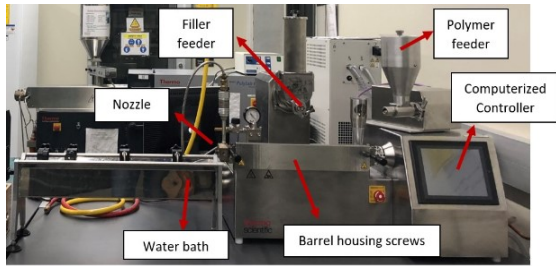
To improve the dispersion of the fillers in the PA12, both components are mixed in a centrifugal planetary Thinky Mixer ARV-310. A 50wt% filler concentration of each composite is loaded at 500 rpm, five cycles of three minutes of mixing and three minutes of resting, and no vacuum. 20 ceramic balls with a diameter of 10mm were added to the containers. These parameters were selected because we wanted to conserve the shape and

size of the magnetic particles. Longer mixing times and different ceramic balls sizes would mill the particles and change the final properties of the composites. Figure 14 shows how the materials change at different stages of the mixing process. The loading levels of magnetic fillers have been gradually increased from 5wt% to 50wt% to study the change in magnetic properties, mechanical behavior and effect during 3D printing. Giving the fact that anisotropy magnets have a larger remanence than isotropy magnets, it is desired to know what the minimum concentration at which optimal magnetic properties are achieved.



**Figure 14.** 50wt% NdFeB/PA12 at zero, two and five mixing cycles of three minutes.

The extrusion process is conducted in a Process 11 Twin Screw Extruder. It has nine temperature zones to gradually melt the materials, mix them and extrude them. The vacuum is applied at stage seven. For all composites, these values were set as follows:  $z_1$ : cool zone,  $z_2$ : 220°C,  $z_3$ : 230°C,  $z_4$ : 230°C,  $z_5$ : 240°C,  $z_6$ : 240°C,  $z_7$ : 240°C,  $z_8$ : 230°C, die: 220°C. This temperature range allowed the composite material to flow continuously. Neat PA12 was extruded with a lower temperature range with the highest temperature at 220°C to avoid thermal degradation. The same path was attempted to produce the composites. However, the viscosity of the new material was too high and increased the torque in the extruder beyond the allowed limit. Consequently, the temperature was increased to avoid damaging the machine and obtain a continuous filament. Figure 15 shows the instrument used and the RPM set at the feeder and screws for each composite.



Material	Feeder RPM	Screws RPM	Filament Diameter [mm]
PA12	55	120	1.55 ± 0.03
OP-71/PA12	50	170	1.3 ± 0.03
OP-56/PA12	30	130	1.3 ± 0.03
NdFeB/PA12	38	140	1.65 ± 0.03

**Figure 15.** Process 11 Twin-Screw Extruder and table showing parameters used to create each composite filament and final diameters.

Note that although different parameters were used for both OP-71/PA12 and OP-56/PA12 filaments, they have the same diameter. Whereas for PA12 and NdFeB/PA12 this value is closer to the 1.75 mm, the preferred filament value. To increase this number, it is recommended to decrease the spooler speed and synchronize it with the screws' rpm, this will allow more material to accumulate in the barrel and will generate the right pressure to extrude more material. However, when the screws rotate at low rpm, warping of the composite at the exit zone occurs. It seems that the magnetic particles are not pulled fast enough away from the die, which causes them to get attracted to it. Additionally, twin screw extruders are characterized for inconsistent filament diameters. This is commonly solved by pelletizing the material and extruding it with a single screw extruder or upgrading the machine with a melt pump [27].

One difficulty during the NdFeB/PA12 extrusion was the fluctuation in pressure that induced a sudden increase of 0.3 mm in the filament diameter, and decrease it again to 1.65 mm. The time or distance at which this effect occurred was not studied. However, Ponsar et al., 2020 attributed this to the accumulation of material in the die, which leads to changes in pressure and die swell [28].



**Figure 16.** Die swell in NdFeB/PA12 filament.

### **2.3. Fused Filament Fabrication**

A CrafBot XL3 was used to print the type I samples required by the ASTM D638 for tension testing, a thickness of 3.25 mm was aimed. The first printed sample had a thickness 0.4 mm larger than the designed one. Therefore, the thickness was adjusted in the CAD file to compensate for such increment. Flexure properties were done following the ASTM D790, a 7 mm x 12.7 mm x 3.25 mm rectangle was designed. These dimensions comply with the specified ones by the ASTM when nose and support rollers have a radius different than 5 mm. The 3D printing of these materials was performed using a 0.4 mm hardened steel nozzle and layer size of 0.2 mm. A temperature of 235°C was intended to use to avoid thermal stresses on the materials but it triggered obstructions several times. Therefore, this parameter was gradually increased to find the optimum value at which all the composites could be printed with no difficulties, this value was found to be 270°C. Additionally, metallic and glass beds heated at 95°C were used to deposit the specimens. However, the first layers did not attach properly and were pushed out of the platform by the nozzle. Therefore, the fans were turned off and glue and paper were needed to guarantee adhesion of the first two layers to the bed, which were printed at 50% speed.

The NdFeB/PA12 samples were successfully obtained without any modification to the 3D printer because of the brittle nature of the filler, which decreased the flexibility of the PA12. Nevertheless, both OP-71/PA12 and OP-56/PA12 composites required the drive gears to be adjusted in the filament feed section to avoid buckling, as can be observed in figure 17. This can be solved by increasing the height of the filament guide or adding a different mount able to contain the filament.

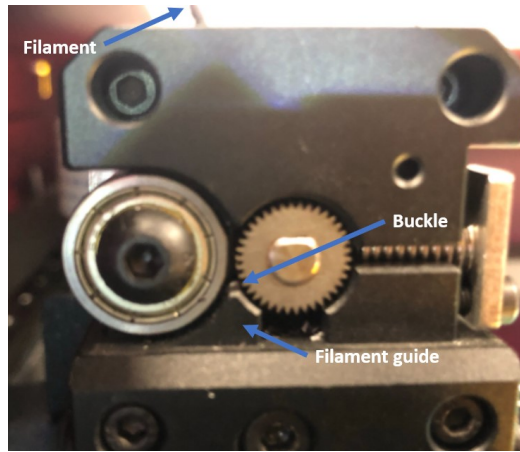


**Figure 17.** CraftBot XL3 feeding zone and OP-56/PA12 buckling between the drive gears.

### 3. CHARACTERIZATION AND RESULTS

#### 3.1. Density measurements

The density of both the composites and neat PA12 was obtained following the ASTM D792. The 5 mm high and 20 mm of radius cylinder shown on the left side of table 2 was printed as the standard requires at least two samples of each material with a volume higher than 1 cm<sup>3</sup> and soft edges.

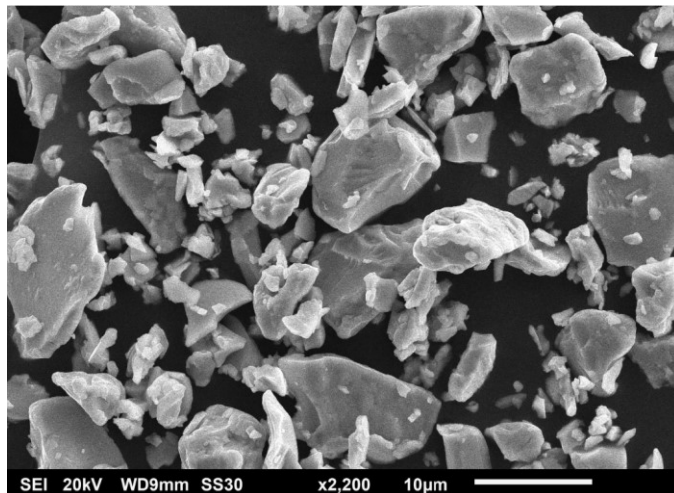
**Table 2.** Density measurements of composites and neat PA12 according to ASTM 792



Density [g/cm <sup>3</sup> ]			
PA12	OP-71/PA12	OP-56/PA12	NdFeB/PA12
1.04	1.40	1.60	1.62

#### 3.2. Scanning Electron Microscope

A JEOL JSM-6010 PLUS/LA SEM is used to observe the different powders, composites, and 3D printed specimens to understand how the alignment of the particles change when they are printed with a magnetic field. To improve resolution, all samples were coated with a 2 nm layer of gold deposited by a Quorum Technologies EMS150T Imaging Sputter Coater.



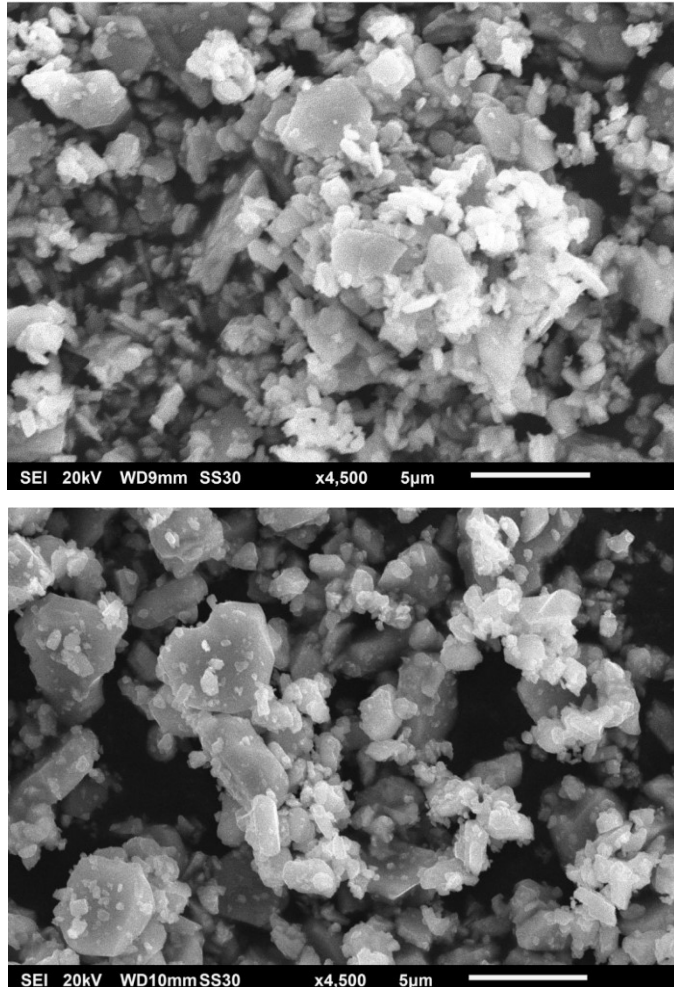


**Figure 18.** NdFeB, OP-56, and OP-71 in powder form.

From figure 18 it can be concluded that the powders used do not have a specific shape. The NdFeB particle range size varies from 5  $\mu\text{m}$  to dimensions as large as 15  $\mu\text{m}$ . OP-51 and OP-56 showed smaller particles of a more consistent size of around 1 – 4  $\mu\text{m}$ . In magnetic materials, the coercivity improves as the particle size decreases [13], and small variations in size are preferred to obtain constant magnetic properties in filled polymers. Moreover, this influences how the composites support the flexure and tension loads.

To analyze the distribution of the particles in PA12, three random samples of each filament were chosen, and different places observed. In figure 19, the first two images

show the NdFeB/PA12 filaments, in which large particles seem to be close to each other and smaller particles are better dispersed. The OP-71/P12 and OP-56/PA12 filaments are shown in the middle and third row of the same figure, the distance between particles is smaller and there seems to be homogeneity despite some larger particles observed. Moreover, the OP-56 powders have a morphological alignment attributed to the extrusion flow.

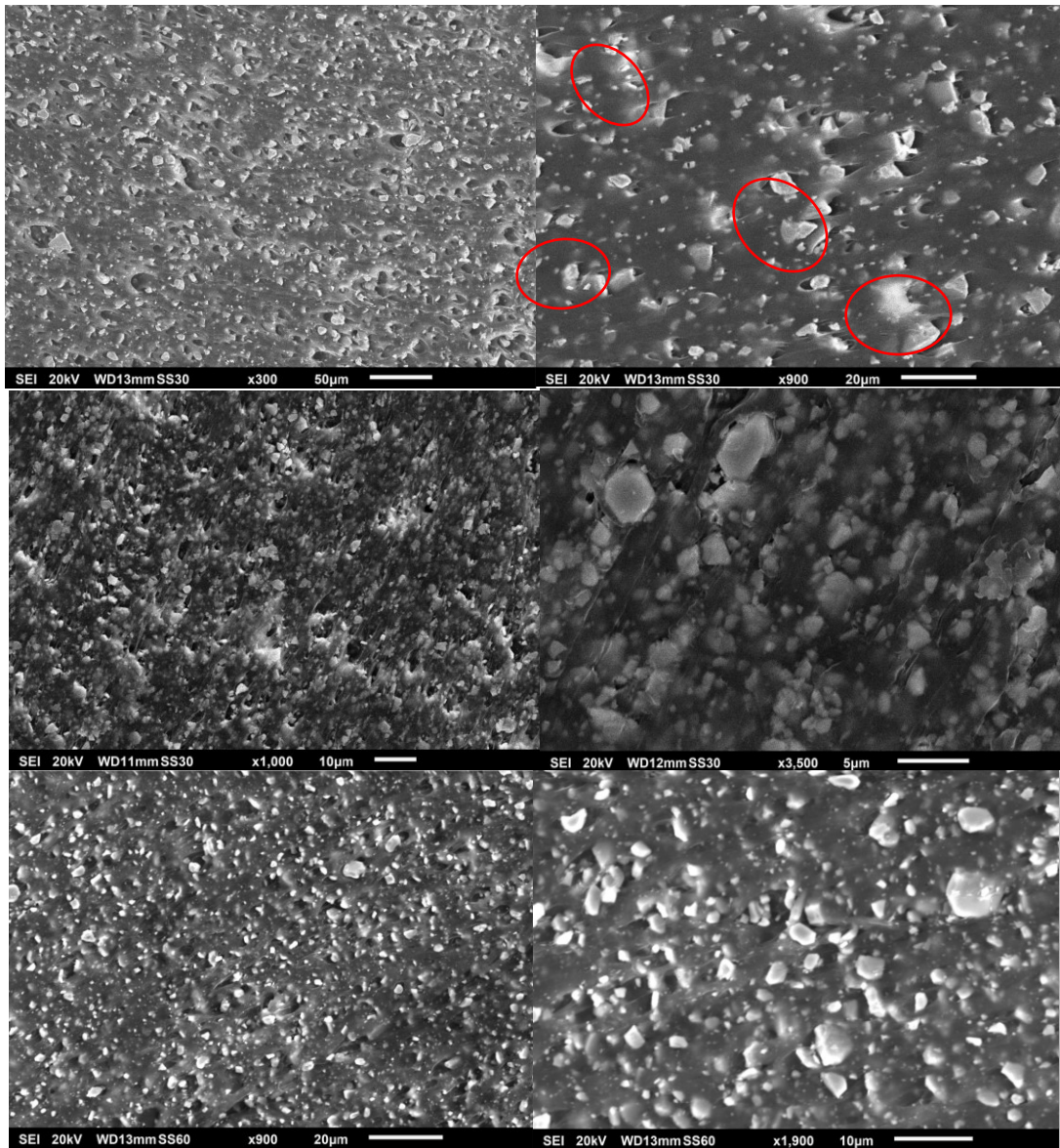


**Figure 19.** NdFeB/PA12 on top, OP-56/PA12 in the middle, and OP-71/PA12 in the last row.

### 3.3. Thermogravimetric Analysis and Differential Scanning Calorimetry

An SDT 650 is used to perform TGA and DSC analyses on the composites and neat PA12. All tests were ramped with a heating rate of 20°C/min up to 600°C in a nitrogen environment. Figure 20 displays the overlay of the thermal analyses on neat PA12, and the composites created. The polymer loses weight in two stages, from 290.4°C to 370°C 1.69%. From that point on, the decomposition occurs at a faster rate leaving a remaining of less than 2% at 588°C. All composites start degrading at around 409°C, stage at which they have decrease 1.4% in average weight compared with 4.8% of neat PA12, indicating an improvement in heat transfer between the matrix and magnetic fillers because of the larger thermal conductivity of the latter during the first degradation stage. Strontium ferrite has been reported to have thermal anisotropy, it transfers the heat through the in-plane direction more efficiently than through the cross section direction [29]. The blue curve corresponds to OP-56/PA12 composites, which starts decomposing at a faster rate reaching a 48% weight loss in the range of 452.7°C to 503°C. The 52% of weight remaining corresponds to the filler and the beginning of the formation of different phases of iron and strontium oxides [30]. A similar behavior is observed with OP-71/PA12, which loses 5% more weight than OP-56/PA12 at 503°C. The brown curve represents NdFeB/PA12, the first decomposition stage is observed to be between 413°C and 453°C. This marks the beginning of a faster weight loss that reaches 45% with temperature increase. The augment emerging from 453°C to 588°C is attributed to corrosion attack, which gives place to oxides such as Fe (II) (FeO) and Fe (III) (Fe<sub>2</sub>O<sub>3</sub>), Nd<sub>2</sub>O<sub>3</sub> and  $\alpha$ -Fe<sub>2</sub>O<sub>3</sub> [31].

Composites show a glass transition at 48.24°C, 44.06°C and 48.91°C of OP-

71/PA12, NdFeB/PA12 and OP-56/PA12, respectively. This is followed by the melting point of PA12 at around 184.1°C in all composites and an exothermic reaction at around 380°C although it happens at a later stage in the NdFeB/PA12 specimen. The melting points of SrFe<sub>12</sub>O<sub>19</sub> are given as 462.94°C and 483°C for OP-56/PA12 and OP-71/PA12, respectively. The melting point of NdFeB is larger than 1000 °C.

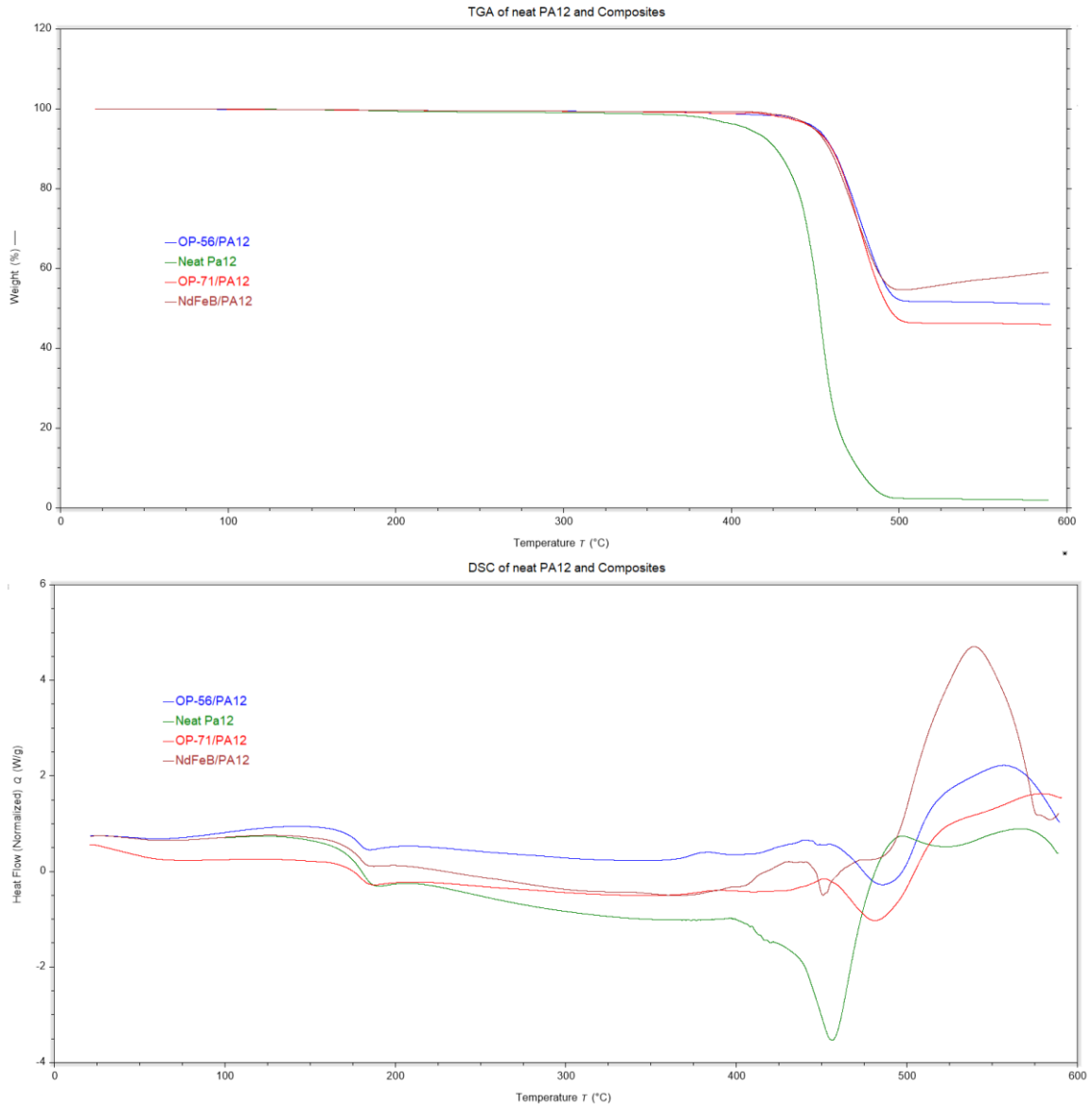


**Figure 20.** TGA and DSC results on neat PA12 and composites with a 50wt% loading level.

### 3.4. Mechanical Properties

Five samples of each composite and neat PA12 were tested under flexure and tension in an Servohydraulic Material Testing System 810 following ASTM D790 and ASTM D638, respectively. There is a minimal decrease in the flexural strength of PA12 when is loaded with 50wt% of SrFe<sub>12</sub>O<sub>19</sub> and NdFeB, and the flexural modulus of OP-56 increases by 7%. In previous studies, at 40wt% of SrFe<sub>12</sub>O<sub>19</sub>/PA12 these properties increased by 18% and 30% respectively. This can be attributed to the different thermal stresses the polymer underwent during extrusion and 3D printing. For instance, at 40wt%, the OP-71/PA12 could be printed at 235°C, while with 10% higher loading level, it requires 35°C more to avoid nozzle obstructions. This temperature is considered high given the fact that PA12 decomposition point starts at around 300°C, according to the manufacturer and TGA results. Additionally, there was a continuous agglomeration in the nozzle of the 3D printer that could reorganize the particle distribution, affecting the final mechanical properties.

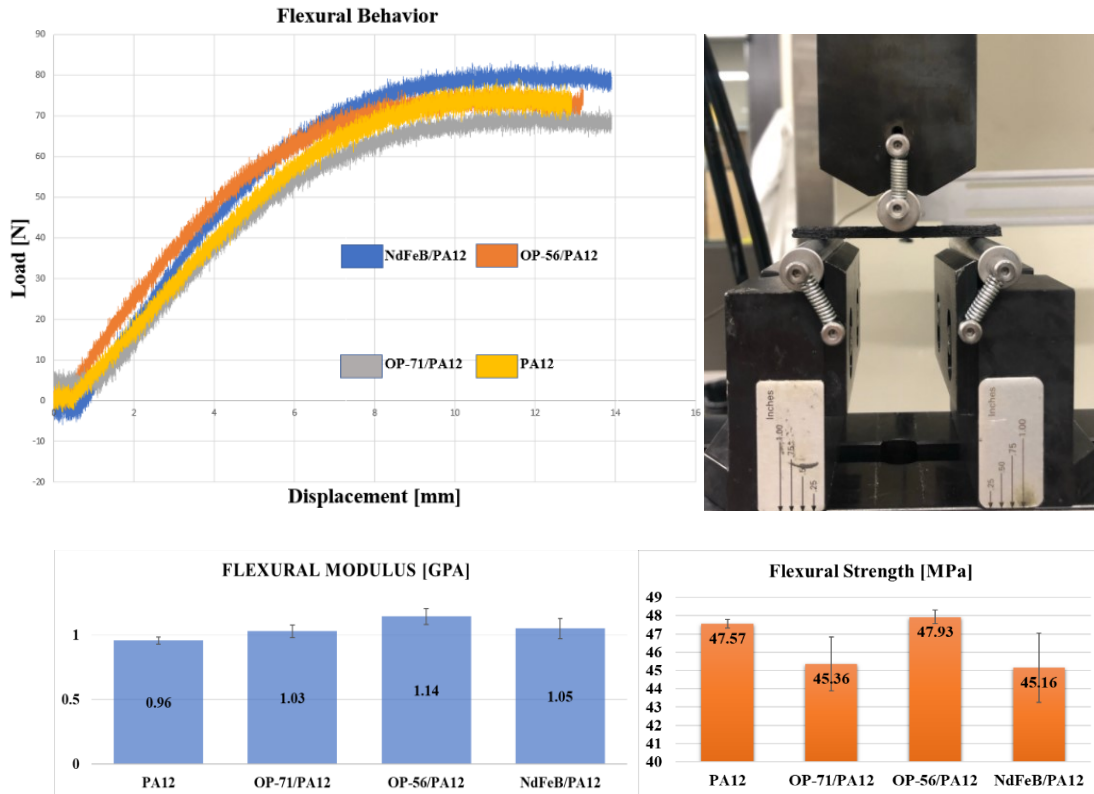


**Figure 21.** Flexural modulus and flexural strength values obtained from the composites manufactured at 50wt% loading levels.

The failure modes at which the composites and neat PA12 failed during tension and the testing set up with an extensometer can be observed in figure 22. Although none of the samples failed inside the grips area, not all ruptures are completely centered. This can be avoided by increasing the thickness of the section that goes inside the grips.

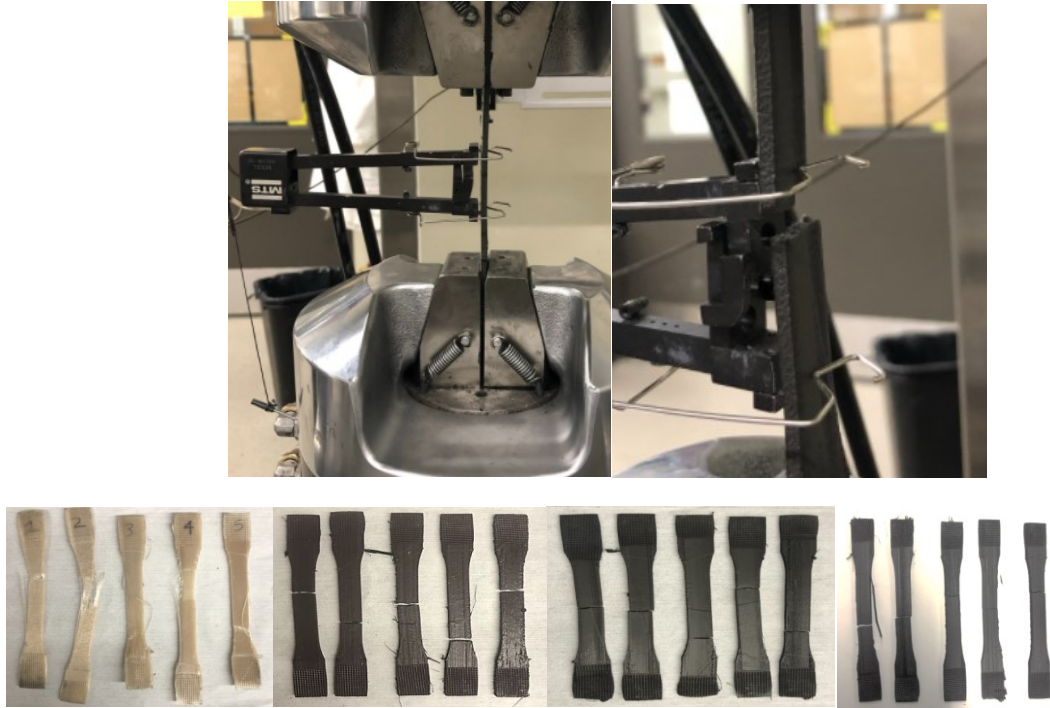


**Figure 22.** Tensile test setting and failure modes of PA12, OP-56/PA12, NdFeB/PA12, and OP-71/PA12.

Regarding the tension properties, all materials yielded at stress-strain values lower than 10 MPa and  $\sim 0.05$  mm/mm. However, their elastic zone continued before strain hardening. The tensile modulus of OP-71/PA12, OP-56/PA12 and NdFeB/PA12 increases by 5.5%, 48.9% and 25.13%, respectively. Therefore, the ability of these materials to resist higher loads is improved before reaching the plastic zone. After this stage, the composites show a brittle behavior and the neat PA12 reaches the necking point. This explains why there are not significant changes in tensile strength, being OP-56/PA12 the only composite showing a slight increase of 6%. The actual effect of these type of load can be seen on figure 20, which also shows the failure modes of both neat PA12 and composites.

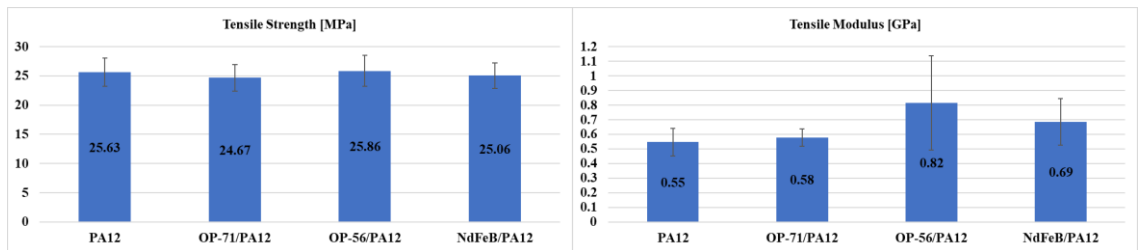
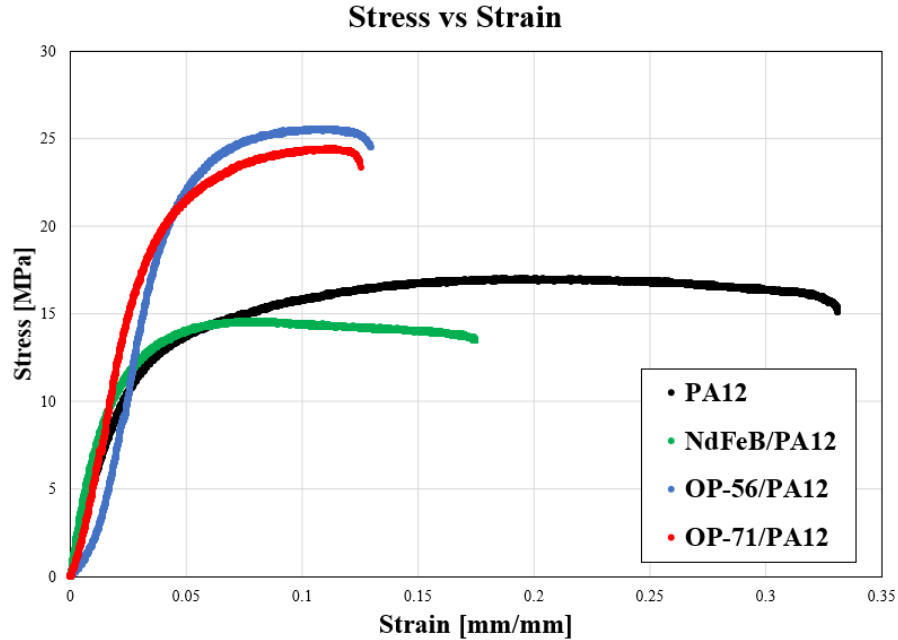


**Figure 23.** Ultimate Tensile strength and tensile modulus.

### 3.5. Magnetic Properties

To determine the magnetic properties of the composite filaments and 3D printed samples, a Microsense LLC / EZ9-HF Vibrator Sample Magnetometer is used. Cylinders with a diameter of 1.25 mm and 15 mm long were 3D printed using the parameters mentioned earlier. To induce the magnetic field, one cubic NdFeB magnets of 24.5 mm and a 5500 Oe perpendicular to the printing direction was attached to a steel plate and placed on top of the bed. This setting, shown in figure 24, contains the magnets from attaching to the extruder.

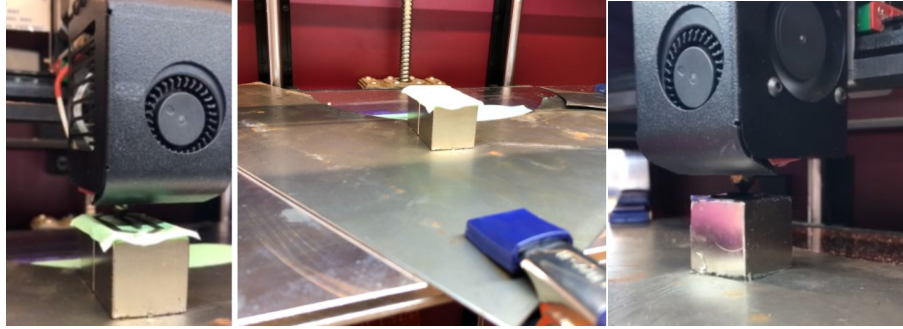
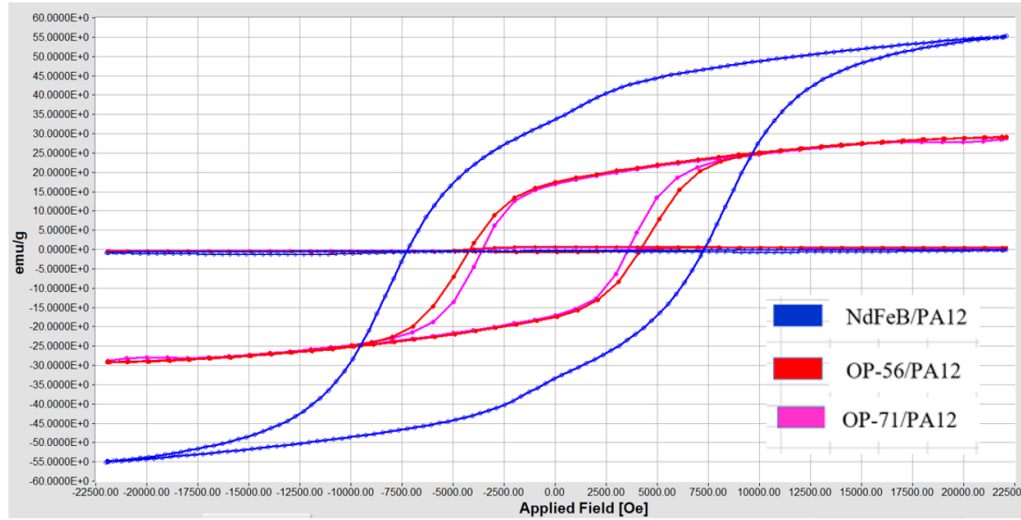


**Figure 24.** Printing set up to induce a magnetic field on magnetic filaments.

In the VSM, the specimens were positioned on a 5 mm perpendicular rod and measurements were done with a sweeping field from -22000 to 22000 at 200 Oe/sec. Additionally, the image and lag effect were corrected. Figure 25 displays the results obtained for the filaments at 50wt% and the table below, the values of saturation ( $M_s$ ), remanence ( $M_r$ ), squareness ( $S$ ) and coercivity ( $H_c$ ) in emu/gram. As expected, NdFeB/PA12 has a larger coercivity compared to that of the strontium ferrite composites. It also has around two times the remanence and saturation values yielded by the OP-71 and OP-56 composites. However, the change in squareness between the three materials does not vary significantly.



Filaments	Ms [emu/g]	Mr [emu/g]	S	Hc [Oe]
OP-71/PA12	18.708	10.906	0.58	3570.572
OP-56/PA12	27.618	16.499	0.60	4185.412
NdFeB/PA12	55.193	33.549	0.61	7259.449

**Figure 25.** Hysteresis loop of filament composites.

Additionally, 3D printed samples with and without a magnetic field were analyzed on the same machine with the same parameters. Compared to the filaments behavior, results show an increase in  $M_s$ ,  $M_r$ ,  $S$  and  $H_c$  in 3D printed specimens when obtained with a 0.4 mm nozzle. Because agglomerations are common in these components with filled materials, samples were printed with a larger nozzle (0.6 mm) to observe how the magnetic properties changed. It must be said that during some experiments, the samples were moved from its initial position on the rod because the particles were being sensitive to the field applied. This caused that, for example, one of the specimens showed more than one easy axis. To solve this issue, the samples being affected were cut to decrease their weight and attach them easier to the holder.



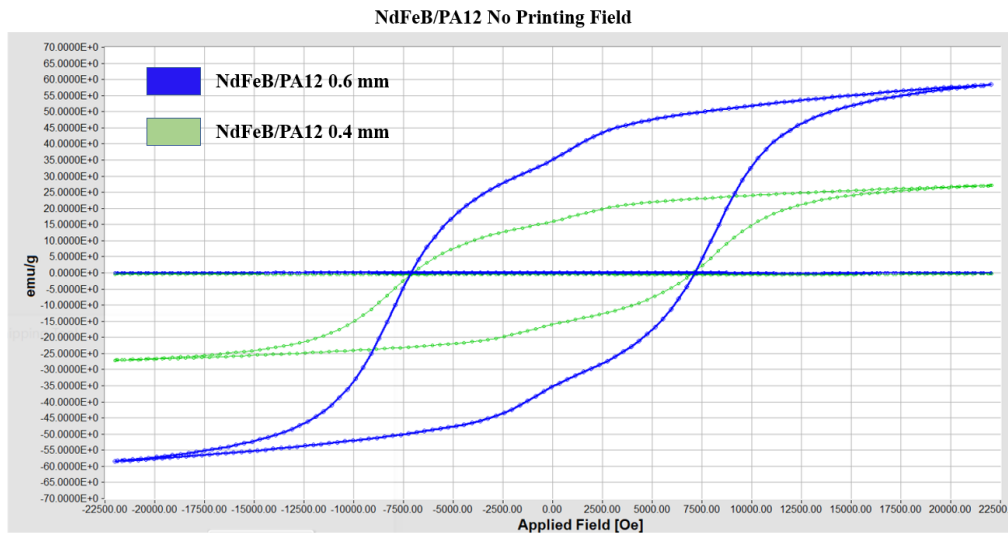
**Figure 26.** Samples on the rod holder. Left, correct position. Right, misaligned position.

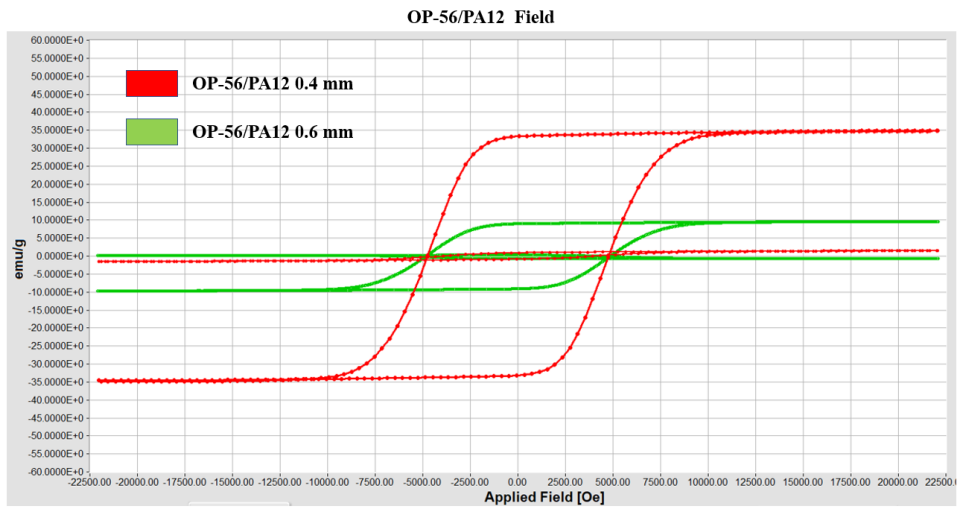
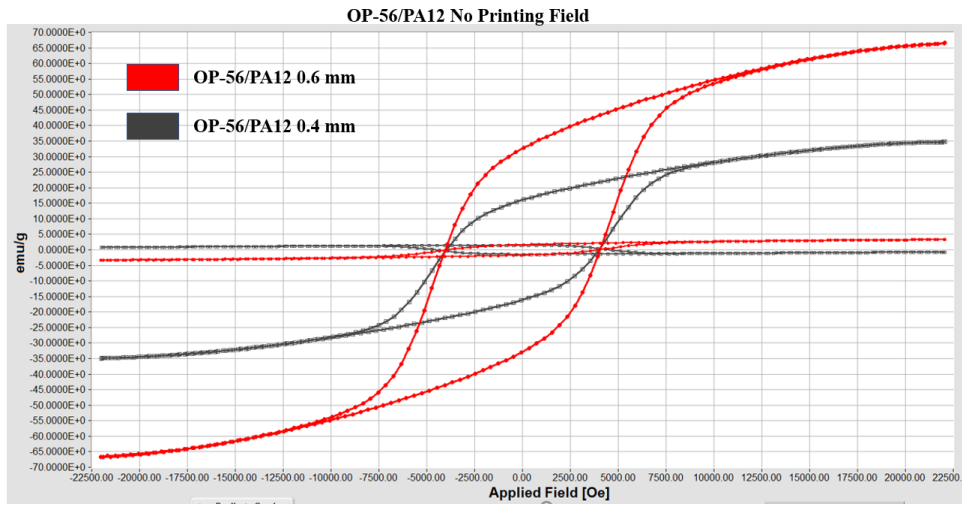
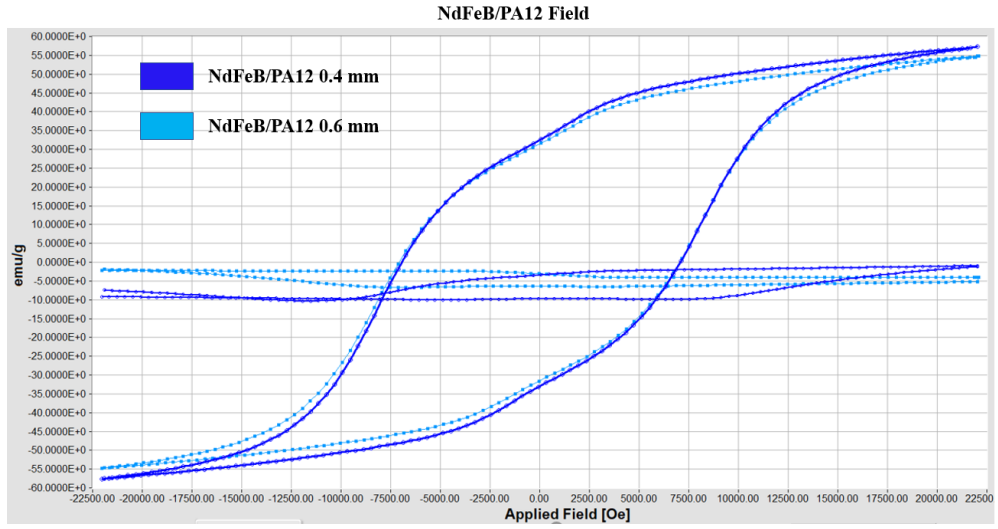
The results are shown in table 3, it can be observed that the  $M_s$  of OP-71/PA12 decreases with the 0.6 mm nozzle, while the NdFeB/PA12 and OP-56/PA12  $M_s$  increases. However, from the data obtained conclusions cannot be made because there is not a trend. Therefore, the changes in the magnetic performance of the materials are attributed to a redistribution of particles when melted again in the extruder. The hysteresis of all materials are shown in figure 27, where the change in squareness can be clearly observed when the samples are printed on top of the NdFeB magnet. However, notice that NdFeB/PA12 3D printed specimens did not saturate at the fields mentioned. Consequently, the same experiment was repeated on a Physical Property Measurement System (PPMS) with a field from -9 Tesla to 9 Tesla. The results at this high fields are displayed on figure 28.

**Table 3.** Saturation ( $M_s$ ), remanence ( $M_r$ ), squareness ( $S$ ) and coercivity ( $H_c$ ) of composites printed with and without the effect of a magnetic field and with two different nozzle sizes.

3D Printed samples 0.4mm nozzle	$M_s$ [emu/g]	$M_r$ [emu/g]	$S$	$H_c$ [Oe]	$M_s$ [emu/g]	$M_r$ [emu/g]	$S$	$H_c$ [Oe]
	No Field				Field			
OP-71/PA12	43.985	21.667	0.49	3443.9	36.138	34.465	0.95	3763.65
OP-56/PA12	33.401	15.410	0.46	3980.8	41.480	39.456	0.95	4758.99
NdFeB/PA12	30.427	17.917	0.59	7044.59	57.514	32.715	0.57	7008.96
3D Printed samples 0.6mm nozzle	$M_s$ [emu/g]	$M_r$ [emu/g]	$S$	$H_c$ [Oe]	$M_s$ [emu/g]	$M_r$ [emu/g]	$S$	$H_c$ [Oe]
	No Field				Field			
OP-71/PA12	30.441	15.142	0.50	3476.15	8.718	8.178	0.94	4835.97
OP-56/PA12	41.625	20.411	0.49	4049.83	17.613	16.972	0.96	3727.89
NdFeB/PA12	33.153	19.926	0.60	7136.08	41.273	23.684	0.57	7058.63

Error	Filaments	Printed samples 0 Oe 0.4	Printed samples 0 Oe 0.6	Printed samples 55 kOe 0.4	Printed samples 55 kOe 0.6
OP-56/PA12	0.449103	0.355	0.462	0.33	0.065
OP-71/PA12	0.473696	0.366	0.226	0.317	0.248
NdFeB/PA12	0.849173	0.447	0.487	0.599	0.436





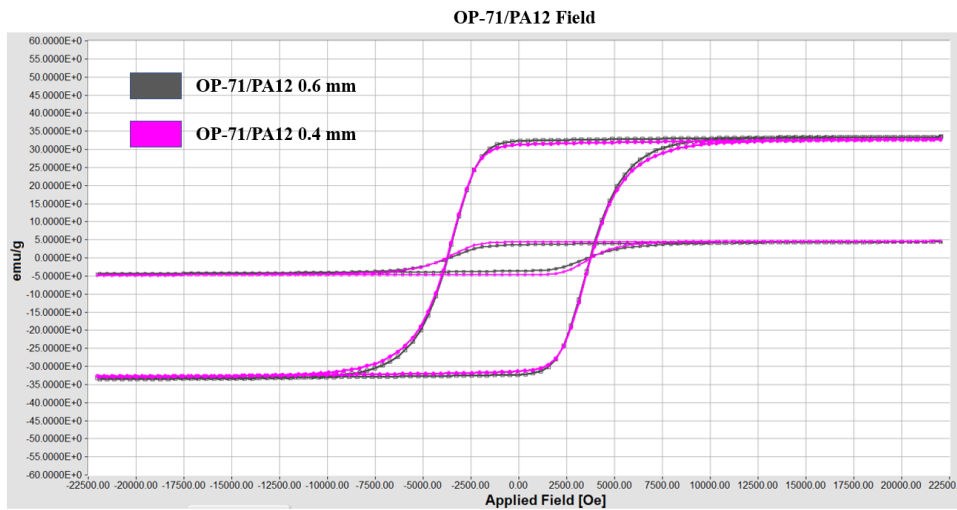
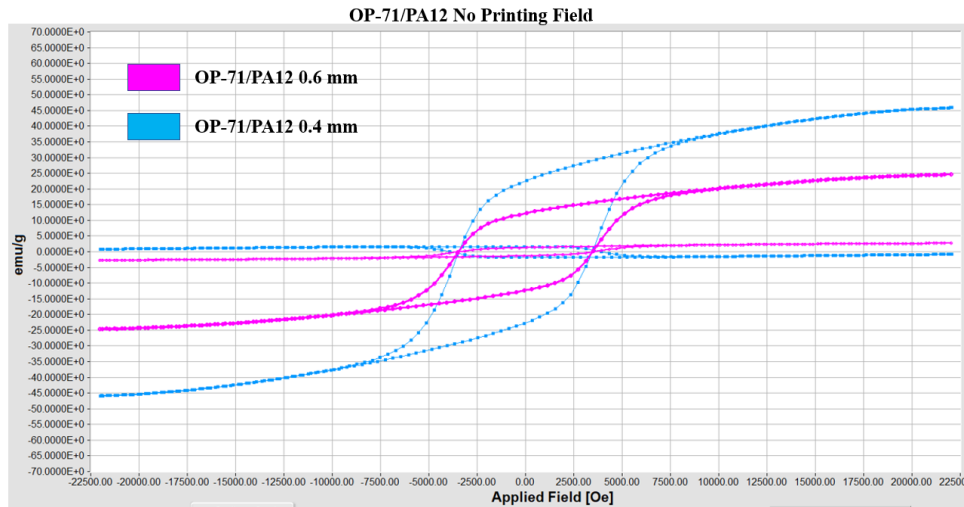


Figure 27. Hysteresis loops of all composites with and without a magnetic field.

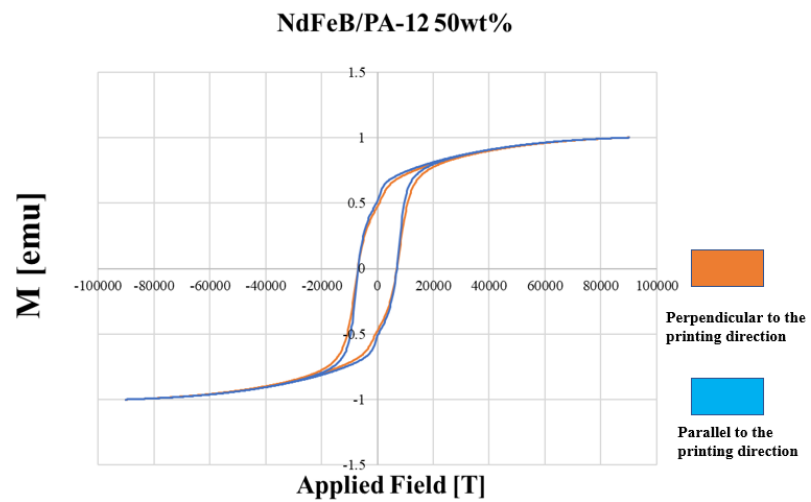
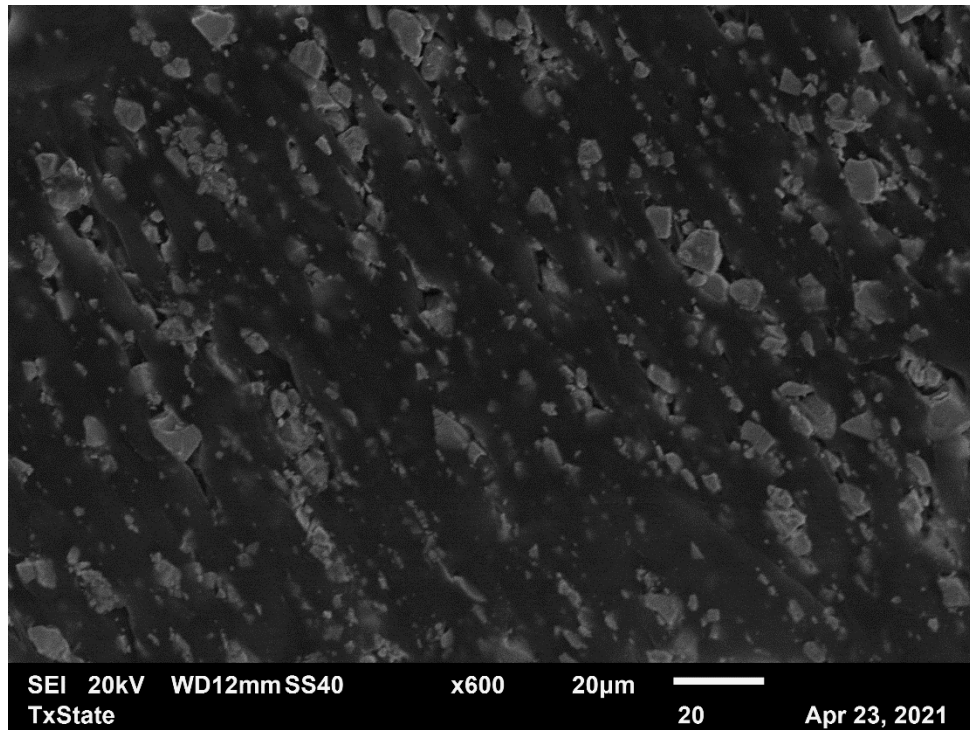
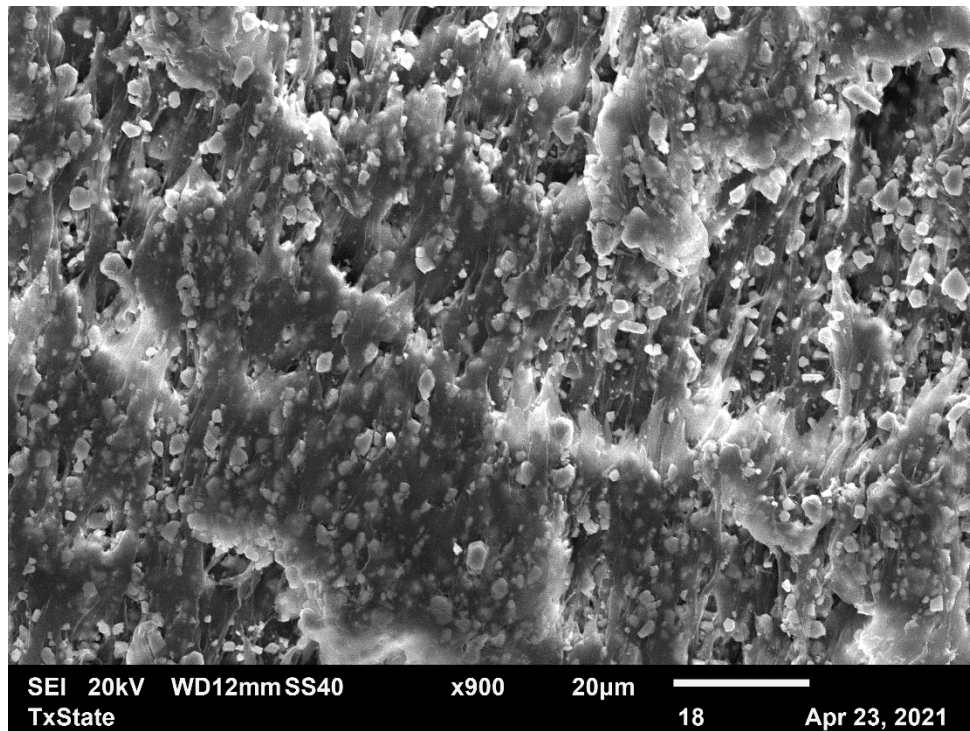
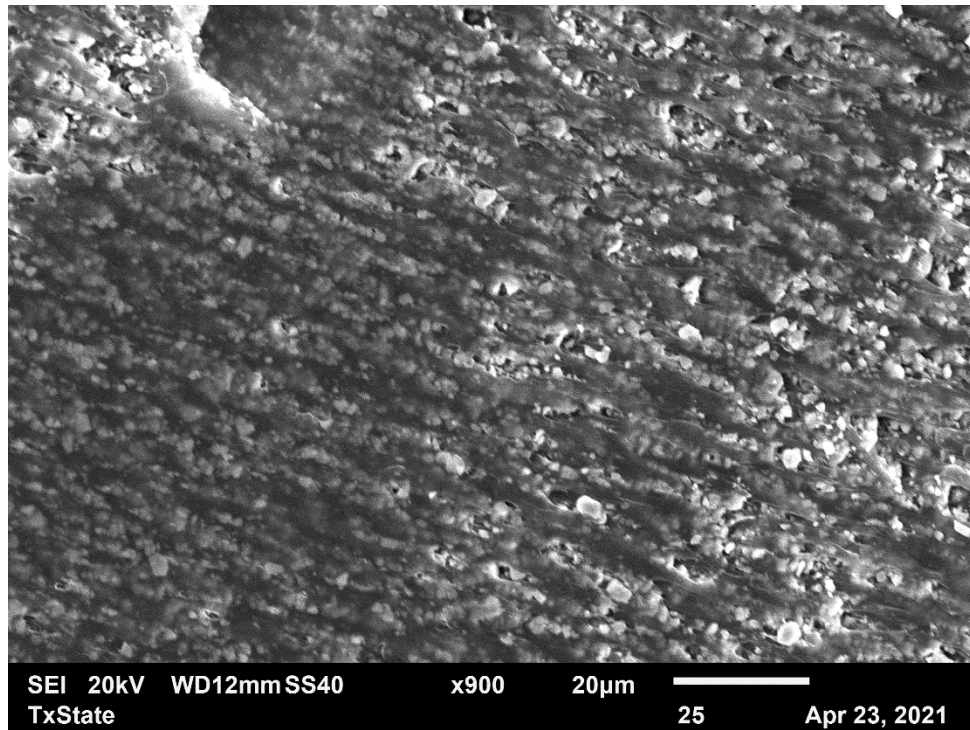


Figure 28. PPMS results of NdFeB/PA12

Additionally, the following SEM images display the morphological alignment of the particles in PA12 when they are printed with the effect of a magnetic field. The first image represents the NdFeB/PA12 composite printed with the effect of a magnetic field, the distance between the chains formed is larger than that seen in the OP-56/PA12, which is below. OP-71/PA12 also shows a tendency to alignment but particles seem to be more dispersed.





**Figure 29.** NdFeB/PA12, OP-56/PA12 and OP-71/PA12 SEM image of particles alignment when the materials are printed with the effect of a magnetic field.

#### 4. CONCLUSIONS

Magnetic filament composites were successfully manufactured using twin screw extrusion. 50wt% of two conventional magnetic materials,  $\text{SrFe}_{12}\text{O}_{19}$  and NdFeB, were added to a Nylon 12 matrix. The temperature range required to obtain the mentioned composites is higher than that of the control material due to the rheology changes when then reinforcements are added. The settings of screws and feeders rpm need to be optimized to eliminate the die swell in the NdFeB/PA12 filaments and increase the diameter in the  $\text{SrFe}_{12}\text{O}_{19}$ /PA12 filaments.

TGA and DSC analyses performed on all the materials show an improved heat flow in the composites compared to that of the neat PA12. Additionally, all the composites show an increase in weight% due probably to the formation of oxides when the magnetic particles reach closer to 500°C.

Samples for mechanical and magnetic tests were successfully obtained using a commercial 3D printer which required a hardened steel nozzle of 0.4 mm. The buckling effect, common in flexible filaments, represented a challenge during the 3D printing of both OP-71 and OP-56 based composites and required the 3D printer to be upgraded. The magnetic results show that there is a potential agglomeration in the extruder section that decreases the filling concentration in the materials. Therefore, a reduction in the magnetic behavior and possibly in the mechanical behavior.

As with the magnetic properties, the OP-56/PA12 filaments displayed a higher flexure and tension behavior. There were no significant changes in tensile strength, but the tensile modulus of NdFeB/PA12, OP-56/PA12 and OP-71/PA12 increased by 5.5%, 48.9% and 25.13%, respectively. The flexural strength is only improved by 6% in

NdFeB/PA12 composites. Additionally, the flexural modulus increased by 7.5%, 19.6% and 9.8% for OP-71/PA12, OP-56/PA12 and NdFeB/PA12, respectively.

The magnetic properties of the filaments and printed materials with and without the effect of a magnetic field were determined. The squareness of all the materials is clearly improved and the morphological alignment is shown in SEM images.

## **5. FUTURE WORK**

Currently, the specimens for magnetic analysis are being printed on top of a magnet to induce a magnetic field and analyze the anisotropy of each material. The implementation of a copper wire solenoid electromagnet attached to the extruder section 3D printer is being developed to saturate the materials. The main challenge to overcome is the overheating produced by the high voltage required from this system. Which limits the size of the specimens printed and the possibility of manipulating the magnetic field to, for example, create hall back arrays.

Additionally, it is essential to determine the exact parameters needed in twin screw extrusion to obtain 1.75 mm filaments to eliminate buckling during 3D printing and obtain samples with the right loading concentration.

## REFERENCES

1. Coetzee, Venkataraman, Militky and Petru. Influence of Nanoparticles on Thermal and Electrical Conductivity of Composites. *Polymers*. 2020. 10.3390/polym12040742
2. Kallagunta and Tate. Low-velocity impact behavior of glass fiber epoxy composites modified with nanoceramic particles. *Journal of Composite Materials*. 2019. 10.1177/0021998319893435
3. Slapnik, Pulko, Rudolf, Anžel and Brunčko. Fused filament fabrication of Nd-Fe-B bonded magnets: Comparison of PA12 and TPU matrices. *Additive Manufacturing*. 2021. <https://doi.org/10.1016/j.addma.2020.101745>
4. Deheri, Swaminathan, Bhame, Liu and Ramanujan. Sol–Gel Based Chemical Synthesis of Nd<sub>2</sub>Fe<sub>14</sub>B Hard Magnetic Nanoparticles. *Chemistry of Materials*. 2010. 10.1021/cm103148n
5. Lewis and Jiménez-Villacorta. Perspectives on Permanent Magnetic Materials for Energy Conversion and Power Generation. *Metallurgical and Materials Transactions A*. 2013. 10.1007/s11661-012-1278-2
6. Huber, Mitteramskogler, Goertler, Teliban, Groenefeld and Suess. Additive Manufactured Polymer-Bonded Isotropic NdFeB Magnets by Stereolithography and Their Comparison to Fused Filament Fabricated and Selective Laser Sintered Magnets. *Materials (Basel, Switzerland)*. 2020. 10.3390/ma13081916
7. Gibson, Rosen and Stucker, *Additive manufacturing technologies: 3D printing, rapid prototyping, and direct digital manufacturing, second edition*. Journal. 2015.
8. Gibson, Rosen and Stucker, *Additive manufacturing technologies: 3D printing, rapid prototyping, and direct digital manufacturing, second edition*. Journal. 2015.

9. Huber, Abert, Bruckner, Grönefeld, Muthsam, Schuschnigg, Sirak, Thanhoffer, Teliban, Windl, Suess and D. 3D print of polymer bonded rare-earth magnets, and 3D magnetic field scanning with an end-user 3D printer. *Applied Physics Letters*. 2016.
10. Huber, Sepehri-Amin, Goertler, Groenefeld, Teliban, Hono and Suess. Coercivity enhancement of selective laser sintered NdFeB magnets by grain boundary infiltration. *Acta Materialia*. 2019. <https://doi.org/10.1016/j.actamat.2019.04.037>
11. Bollig, Patton, Mowry and Nelson-Cheeseman. Effects of 3D Printed Structural Characteristics on Magnetic Properties. *IEEE Transactions on Magnetics*. 2017. 10.1109/TMAG.2017.2698034
12. Horák, Babič, Macková and Beneš. Preparation and properties of magnetic nano- and microsized particles for biological and environmental separations. *Journal of Separation Science*. 2007. 10.1002/jssc.200700088
13. Mørup, Hansen and Frandsen, Andrews, Scholes and Wiederrecht, 1.14 - Magnetic Nanoparticles. Amsterdam: Academic Press, Journal. 2011.
14. Lagorce and Allen. Magnetic and mechanical properties of micromachined strontium ferrite/polyimide composites. *Journal of Microelectromechanical Systems*. 1997. 10.1109/84.650127
15. Ketov, Yagodkin and Menushenkov. Structure and magnetic properties of strontium ferrite anisotropic powder with nanocrystalline structure. *Journal of Alloys and Compounds*. 2011. <https://doi.org/10.1016/j.jallcom.2010.09.184>
16. B. D. Cullity and Graham, *Magnetic Anisotropy*. Journal. 2008.
17. Granados-Miralles, Saura-Múzquiz, Bøjesen, Jensen, Andersen and Christensen. Unraveling structural and magnetic information during growth of nanocrystalline SrFe<sub>12</sub>O<sub>19</sub>. *Journal of Materials Chemistry C*. 2016. 10.1039/C6TC03803D

18. Hanemann, Syperek and Nötzel. 3D Printing of ABS Barium Ferrite Composites. *Materials* (1996-1944). 2020. 10.3390/ma13061481
19. Shrivastava, Shrivastava, 5 - *Plastics Processing*. William Andrew Publishing, Journal. 2018.
20. Huber, Cano, Teliban, Schuschnigg, Groenefeld and Suess. Polymer-bonded anisotropic SrFe<sub>12</sub>O<sub>19</sub> filaments for fused filament fabrication. *Journal of Applied Physics*. 2020. 10.1063/1.5139493
21. Hu, Lum, Mastrangeli and Sitti. Small-scale soft-bodied robot with multimodal locomotion. *Nature*. 2018. 10.1038/nature25443
22. Iqbal, Khatoon, Kotnala and Ahmad. Mesoporous strontium ferrite/polythiophene composite: Influence of enwrappment on structural, thermal, and electromagnetic interference shielding. *Composites Part B: Engineering*. 2019. <https://doi.org/10.1016/j.compositesb.2019.107143>
23. Kallaste, Kilk, Belahcen, Vaimann and Janson, Demagnetization in Permanent Magnet Slotless Generator Using Halbach Array. *Journal*. 2012.
24. Bollig, Hilpisch, Mowry and Nelson-Cheeseman. 3D printed magnetic polymer composite transformers. *Journal of Magnetism and Magnetic Materials*. 2017. <https://doi.org/10.1016/j.jmmm.2017.06.070>
25. Zakaria, Abd, Abd, Haroun, Elfaki and Elgani, Explanation of the Effect of Magnetic Field on laser Intensity on the Basic of Generalized Special Relativity. *Journal*. 2014.
26. Verma, Pandey and Sharma. Strontium ferrite permanent magnet - An overview. *Indian Journal of Engineering and Materials Sciences*. 2000.

27. Martin, Repka, Langley and DiNunzio, Twin Screw Extrusion for Pharmaceutical Processes. New York, NY: Springer New York, Journal. 2013.
28. Ponsar, Wiedey and Quodbach. Hot-Melt Extrusion Process Fluctuations and their Impact on Critical Quality Attributes of Filaments and 3D-printed Dosage Forms. *Pharmaceutics*. 2020. 10.3390/pharmaceutics12060511
29. Volodchenkov, Ramirez, Samnakay, Salgado, Kodera, Balandin and Garay. Magnetic and thermal transport properties of SrFe<sub>12</sub>O<sub>19</sub> permanent magnets with anisotropic grain structure. *Materials & Design*. 2017. <https://doi.org/10.1016/j.matdes.2017.03.082>
30. González, Parga, Moreno, Ramos, Martínez, Martínez and Vazquez. Synthesis and Characterisation of Strontium Hexaferrite Using an Electrocoagulation by-Product. *Journal of Chemical Research*. 2016. 10.3184/174751916X14533976548491
31. Pigliaru, Rinaldi, Ciccacci, Norman, Rohr, Ghidini and Nanni. 3D printing of high performance polymer-bonded PEEK-NdFeB magnetic composite materials. *Functional Composite Materials*. 2020. 10.1186/s42252-020-00006-w